

Impact of land surface processes on convection over West Africa in convection-permitting ensemble forecasts: A case study using the MOGREPS ensemble

Valiyaveetil Shamsudheen Semeena¹  | Cornelia Klein^{1,2} |
Christopher M. Taylor^{1,3}  | Stuart Webster⁴

¹UK Centre for Ecology and Hydrology, Wallingford, UK

²Department of Atmospheric and Cryospheric Sciences, University of Innsbruck, Innsbruck, Austria

³National Centre for Earth Observation, Wallingford, UK

⁴UK Met Office, Exeter, UK

Correspondence

Valiyaveetil Shamsudheen Semeena, UK Centre for Ecology and Hydrology, Wallingford OX10 8BB, UK.
Email: semval@ceh.ac.uk

Funding information

Global Challenges Research Fund, Grant/Award Numbers: NE/P021077/1, NE/W001888/1; Natural Environment Research Council LMCS project

Abstract

Soil moisture (SM) affects weather through its impact on surface flux partitioning, influencing vertical atmospheric profiles and circulations driven by differential surface heating. In West Africa, observational studies point to a dominant negative SM-precipitation feedback, where dry soils help to initiate and maintain convection. In this context, serious concerns exist about the ability of models with parameterised convection to simulate this observed sensitivity of daytime convection to SM. Here, we evaluate the effect of initial SM perturbations in a short-range ensemble forecast over West Africa, comparing the UK Met Office Global and Regional Ensemble Prediction System (MOGREPS) with parameterised convection (GLOB-ENS) to its regional convection-permitting counterpart (CP-ENS). Results from both models suggest SM perturbations introduce considerable spread into daytime evaporative fraction (EF) and near-surface temperatures. This spread is still evident on Day 3 of the forecast. Both models also show a tendency to increased afternoon rainfall frequency over negative EF anomalies, reproducing the observed feedback. However, this effect is more pronounced in CP-ENS than GLOB-ENS, which illustrates the potential for process-based forecast improvements at convection-permitting scales. Finally, we identify persistent biases in rainfall caused by land cover mapping issues in the operational GLOB-ENS setup, emphasising the need for careful evaluation of different mapping strategies for land cover.

KEYWORDS

convection-permitting, ensemble forecast, land-atmosphere interaction, rainfall, soil moisture

This is an open access article under the terms of the [Creative Commons Attribution](https://creativecommons.org/licenses/by/4.0/) License, which permits use, distribution and reproduction in any medium, provided the original work is properly cited.

© 2023 The Authors. *Atmospheric Science Letters* published by John Wiley & Sons Ltd on behalf of the Royal Meteorological Society.

1 | INTRODUCTION

In the tropics, the skill of Numerical Weather Prediction (NWP) is known to be considerably poorer than at mid-latitudes. Analysing a handful of global NWP models, Haiden et al. (2012) found levels of skill in predicting 1-day tropical rainfall broadly similar to 6-day rainfall forecasts at higher latitudes, and levels of skill appear to be particularly low over Africa (Vogel et al., 2020). Based on outputs over northern Tropical Africa from 10 global NWP ensemble prediction systems, Vogel et al. (2018) demonstrated that precipitation forecasts there are generally no better than climatology, even after statistical post-processing.

One key reason for the poor forecasting skill over tropical Africa is that the weather is dominated by organised convective storms (Zipser et al., 2006), with the synoptic scale exerting weak forcing compared to mid-latitudes. Moreover, current global ensemble prediction systems rely on convective parameterisations to represent storms. These have well-known biases, tending to produce rain that is too light, too frequent, and too disorganised (Stephens et al., 2010), and are deemed to be a “potential cause for the sobering lack of ensemble forecast skill in a region dominated by mesoscale convective systems” (Vogel et al., 2018).

However, the need for reliable weather forecasting over Africa is high, with a primarily rain-fed agricultural sector and often low resilience to hazardous weather. The African Science for Weather Information and Forecasting Techniques (SWIFT) project (Parker et al., 2022) was an international effort to improve African weather forecasting capacities on time scales from hours out to several months. Within a SWIFT pilot testbed (cf., Fletcher et al., 2022), the UK Met Office for the first time trialled regional convection-permitting (CP) ensemble forecasts for tropical Africa, nested within their operational UK Met Office Global and Regional Ensemble Prediction System (MOGREPS-G Bowler et al., 2008). The CP ensemble (CP-ENS) explicitly captures the convective events that dominate African rainfall, thus, overcoming many issues in the representation of organised convection Crook et al. (2019); Martínez and Chaboureau (2018), which plague coarse-scale forecast models that rely on convective parameterisations. To date, there is no operational use of short-range CP ensembles for African weather forecasting and only few experimental studies, which however suggested that explicit treatment of convection can affect wave propagation speeds (Torn, 2010) and improve ensemble spread and ameliorate underdispersion (Maurer et al., 2017) over West Africa. For the SWIFT testbed, Cafaro et al. (2021) have already shown that CP-ENS over East Africa is significantly more skillful in predicting heavy rainfall than MOGREPS-G.

In this study, we take advantage of these unique CP-ENS trial simulations to evaluate how the land surface representation affects temperature and rainfall

forecasts over West Africa, comparing this aspect to the operational global forecast ensemble. Our focus on West Africa for this study is motivated by a well-documented strong sensitivity of rainfall to soil moisture (SM) and land surface fluxes in this region (Koster et al., 2004; Taylor et al., 2012). In this moisture-limited regime, availability of SM controls surface flux partitioning, which affects the properties of the Planetary Boundary Layer (PBL) and convective instability.

Previous studies of precipitation forecasts in the region have already emphasised the importance of SM initialisation (Agustí-Panareda et al., 2010; Maurer et al., 2015), where a more realistic representation of SM may provide predictability of where storms will trigger (Birch et al., 2014). In practice, this predictability is difficult to realise because of poor observational constraints for SM states (Agustí-Panareda et al., 2010), biases in modelled land-atmosphere processes when convection is parametrised (Hohenegger et al., 2009; Taylor et al., 2012) and our limited knowledge of spatial surface flux structures on any particular day due to the transient nature of SM (Taylor, Parker, et al., 2011). Accounting for uncertainties in initial SM states has generally been found to be important to reduce ensemble forecast overconfidence in near-surface atmospheric states (Tennant & Beare, 2014). We expect such effects to be particularly pronounced for West Africa, making it an ideal test case to explore simulated land-atmosphere interaction effects on the ensemble forecasts. Indeed, Maurer et al. (2015) found that the effectiveness of SM perturbations in generating ensemble spread is as large as the effectiveness of atmospheric perturbations in West Africa. However, their introduced perturbations were external; linked to choices in soil physics, parameters within land surface schemes and remotely sensed as well as model-derived SM fields.

Here, we consider an ensemble forecast system where SM perturbations are created internally, occurring from the natural rainfall evolution in individual ensemble members, thus reflecting physically more realistic SM perturbations (Tennant & Beare, 2014). We explore the impact of land-atmosphere interactions in a MOGREPS forecast created by the UK Met Office during a SWIFT forecasting pilot testbed for April 2019, comparing CP-ENS with its parent global forecast model. This allows us to illustrate for the first time how model-consistent ensemble spread in SM affects forecast spread in a land-atmosphere interaction hotspot.

2 | DATA AND METHODOLOGY

2.1 | Model description

We use ensemble simulations based on the operational MOGREPS-G, and a nested, regionally downscaled

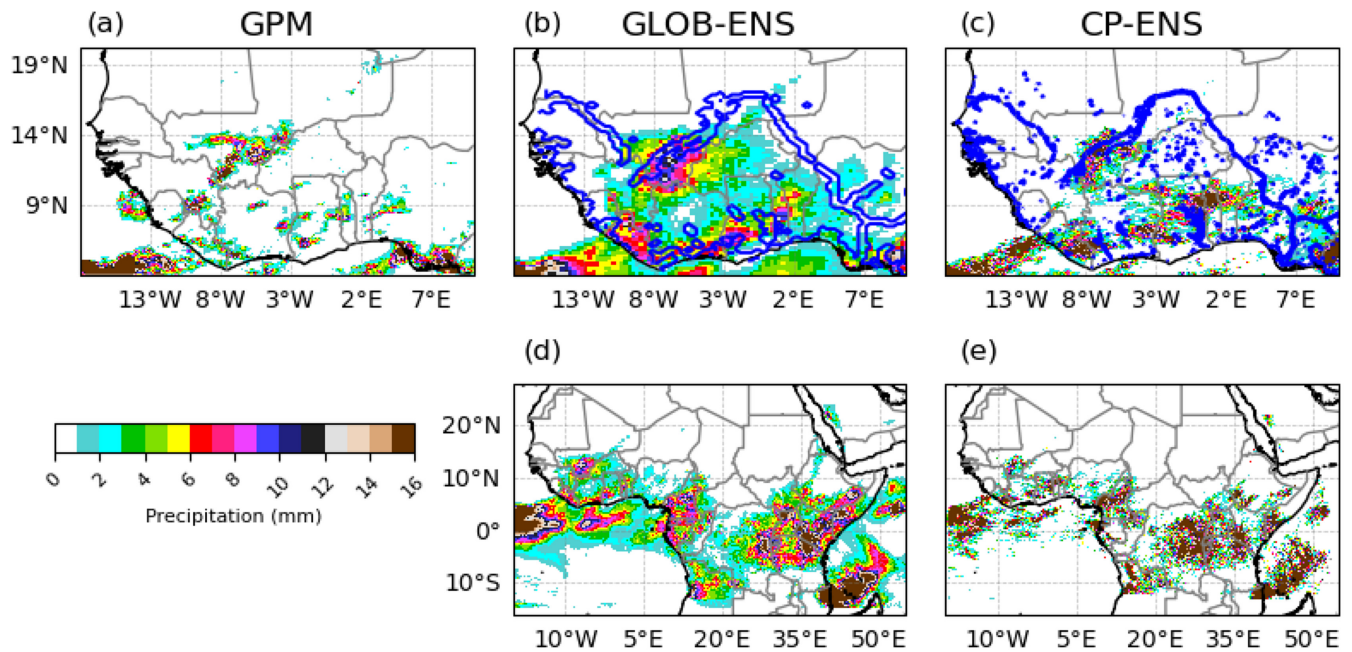


FIGURE 1 Daily accumulated precipitation ($\text{mm}\cdot\text{day}^{-1}$) in IMERG observations (a), and ensemble mean forecasts for GLOB-ENS (b) and CP-ENS (c) for 25th April 2019, forecast-day 1. Blue contours represent the inland water fraction (50%). (d, e) same as (b,c), but for the entire simulation domain of the respective models.

counterpart based on MOGREPS-UK (Hagelin et al., 2017) with some adaptations for the tropical African domain as described in Cafaro et al. (2021) for tropical East Africa. The ensemble forecast trial over West Africa was performed as part of a SWIFT Pilot Testbed (Fletcher et al., 2022) over the period 19th April to 12th May 2019. The nested convection-permitting ensemble (CP-ENS) with a domain centred on West Africa (Figure 1e) was run with 80 vertical levels with a model top level at 38.5 km and at a horizontal grid spacing of 0.08° (8.8 km). The land and atmosphere physics and dynamics schemes used for the tropical regions are explained in Bush et al. (2020) and Porson et al. (2019). A limited area cut out of MOGREPS-G (hereafter GLOB-ENS) spanning the same area as CP-ENS (Figure 1d) was run using the MOGREPS-G setup and resolution (0.28° longitude \times 0.1875° latitude), but excluding stochastic physics perturbations. This ensured that differences in the GLOB-ENS members are solely down to the initial conditions and thus the same as for the CP-ENS ensemble.

Within the model, land surface fluxes and properties are described by the Joint UK Land Environment Simulator (JULES, Best et al., 2011). Each grid point is split into tiles representing different plant functional types (e.g., broadleaf tree, C3 and C4 grasses, shrubs) and non-plant tiles including bare soil and open water. Over each tile, a surface energy budget is solved, based on tile-specific parameters such as leaf area index, albedo and roughness length, and turbulent fluxes are weighted by tile fraction to provide gridbox mean fluxes to the

atmosphere. The latent heat flux is comprised of transpiration, canopy interception, and bare soil evaporation. The latter is controlled by volumetric SM in the top soil layer (10 cm) via a conductance term which is a function of $(SM/SM_{crit})^2$, where SM_{crit} is a texture-dependent soil parameter below which transpiration becomes limited by SM, and is derived for each gridbox from global soil maps Bush et al. (2020). Fractional tile coverage in GLOB-ENS is derived from an IGBP classification while CP-ENS uses the ESA CCI land cover product Bush et al. (2020). Differences between the two maps are discussed in Section 3.

Both GLOB-ENS and CP-ENS consist of 17 perturbed members and one control member for which simulations are run for up to 72 h (3 days), initialized four times a day (at 0000, 0600, 1200 and 1800 UTC). In this study, we use the 0000 UTC simulation starting on 25 April 2019, corresponding to a forecast that captured an extreme rainfall event that was reportedly associated with flooding over Western Mali. All analyses focus on the ensemble response to initial perturbations on Day 1 of the forecast if not otherwise stated, considering surface fluxes and atmospheric states only from 0600 UTC and thus allowing 6 h of spin-up time (e.g., Ma et al., 2021).

Members within MOGREPS are created by applying the ensemble transform Kalman filter data assimilation scheme (Bowler et al., 2008) to thermodynamic and dynamic variables (Tennant, 2015). Following Tennant and Beare (2014), a physically based method is used to introduce spread in SM, and comes as a consequence of the

members' diverging rainfall patterns: For MOGREPS-G, SM perturbations are inherited from the previous forecast cycle by extracting the ensemble mean from naturally evolved SM changes per member, and resulting SM perturbations are added to the SM field of the subsequent deterministic model analysis to recreate SM spread. The initial conditions for both CP-ENS and GLOB-ENS are created by downscaling these initial conditions of the corresponding MOREPS-G member, such that each pair across the two ensembles effectively shares the same initial atmospheric and SM perturbations. with checks to avoid values exceeding physical limits (wilting point and saturation level). The initial conditions for both CP-ENS and GLOB-ENS are created by downscaling these initial conditions of the corresponding MOGREPS-G member, such that each pair across the two ensembles effectively shares the same initial atmospheric and SM perturbations. In this study, we examine how the introduced perturbations in initial SM across the ensembles impact on land-atmosphere fluxes and the atmosphere.

We diagnose the simulations using accumulated precipitation and 1.5 m temperature output every hour, and 3-h mean surface fluxes, and net shortwave radiation. We use the evaporative fraction (EF), defined as the ratio of latent to sensible plus latent heat, to quantify surface flux partition. For the ensemble intercomparison, all CP-ENS variables are regridded onto the GLOB-ENS grid. If not otherwise stated, all analyses focus on the first day of the forecast when initial SM perturbation will affect the atmosphere before decaying over time.

2.2 | Observational data

We compare forecast precipitation with estimates derived from merged satellite and gauge data provided by the Integrated Multi-satellite Retrievals for GPM Huffman et al. (2019, IMERG). We also show daily mean land surface temperature (LST) data sampled on 25th April 2019, based on retrievals at approximately 3 km resolution from the Spinning Enhanced Visible and Infra-Red Imager (SEVIRI) on board Meteosat Second Generation satellites (LSA SAF, 2019; Sobrino & Romaguera, 2004). The 15 min interval near-real-time LST data between 0700 and 1700 h of the day is used for the daytime mean calculation.

3 | RESULTS

3.1 | Summary of rainfall forecast and effect of land surface classifications

Comparison of observed and modelled daily mean rainfall in Figure 1 illustrates that both ensembles were overall

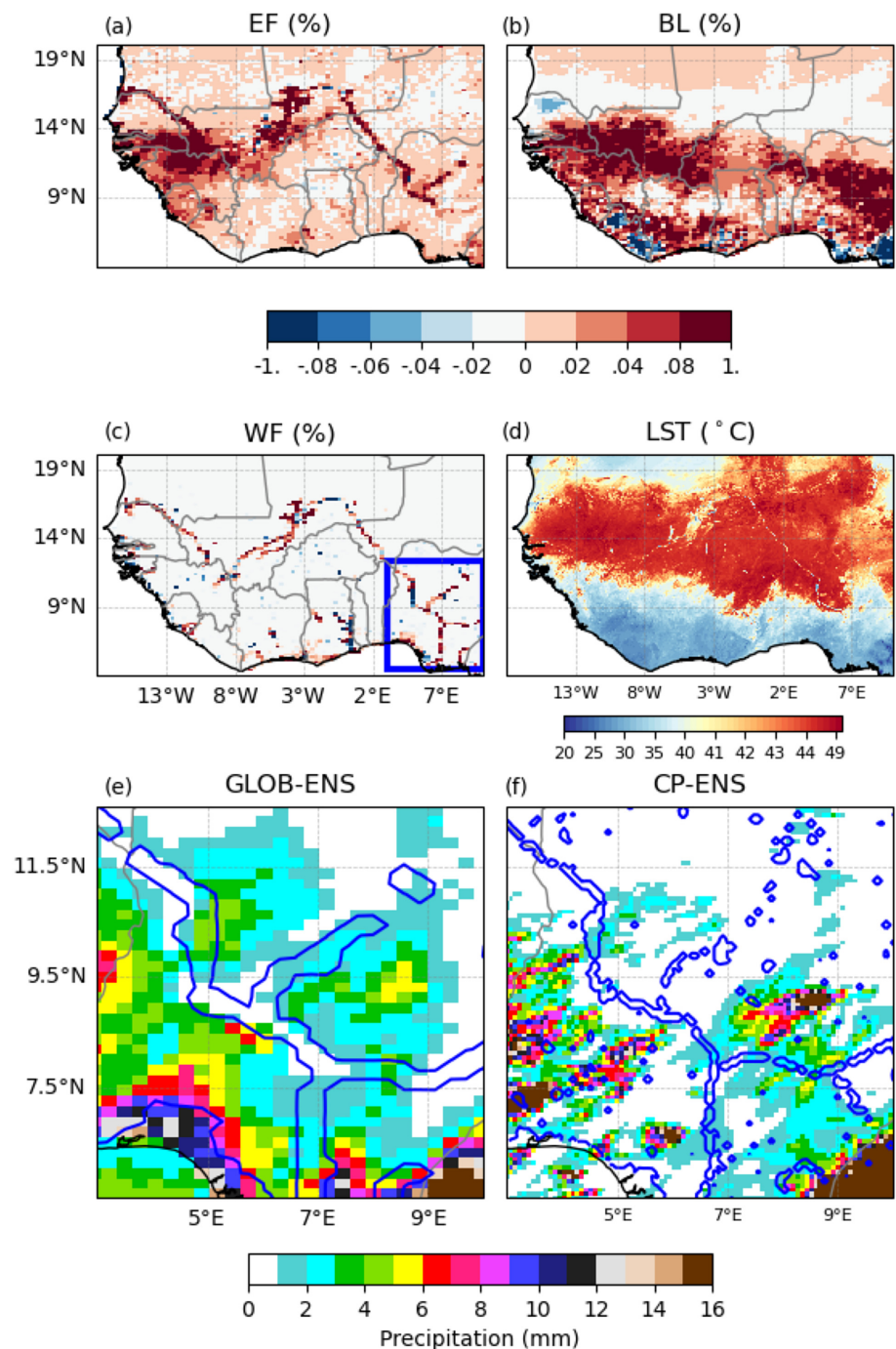
able to forecast the heavy rain that was observed over southeastern Mali, as well as more scattered convection across southern West Africa. GLOB-ENS however shows typical characteristics of parameterised convection, with widespread light- to medium-intensity rain compared to CP-ENS, which produces more discrete, heavily precipitating convective cells (cf. Figure 1b,c). Nevertheless, both GLOB-ENS and CP-ENS show strong consistency across ensemble members in the positioning of the large convective event in the upper Niger catchment with a maximum of 13 (72% in CP-ENS) to 18 members (100% in GLOB-ENS) producing significant morning rainfall in the area (Figure S1a,b), suggesting strong synoptic forcing.

As well as differences in their representation of convection, the two ensembles have alternative fractional cover of land types. These differences give rise to contrasting patterns of ensemble mean EF (Figure 2a). Higher values of EF ~ 0.1 in the western Sahel in GLOB-ENS are due to Broadleaf Tree coverage several 10 s of percent higher in its IGBP-based classification compared to the ESA CCI-derived version used in CP-ENS (Figure 2b). There are also fine-scale structures corresponding to the Senegal and Niger Rivers where remarkably large EF differences ~ 0.4 are found. These are due to different approaches to mapping water bodies in the two ensembles (Figure 2c). In this case, a comparison with Land Surface Temperature observations at 3 km (Figure 2d) identifies which model is in error. There are stretches of these rivers which are wide enough to be visible in the LST map, but it is clear that the fractional cover of rivers in GLOB-ENS, which in places reaches upto 80%, is grossly exaggerated. The impact of this artificial mesoscale flux heterogeneity on rainfall around the Niger in Nigeria can be seen in Figure 2e. The pattern of accumulated rain over the 3-day forecast exhibits a strong suppression over the erroneously wide Niger River in GLOB-ENS, a feature not simulated in CP-ENS, with its more realistic surface forcing. Such suppression of rain is widely observed across larger African wetlands (Taylor et al., 2018), associated with surface-induced mesoscale circulations.

3.2 | Atmospheric response to initial SM perturbations

Here, we explore the relationships between top-level SM perturbations, surface flux partitioning, air temperatures and afternoon rainfall across ensemble members. The rainfall response to the initial SM state and associated EF will strongly depend on the environmental conditions needed to trigger convection in the two models, affecting local rainfall probabilities. Due to the simultaneously introduced atmospheric and SM perturbations, we cannot

FIGURE 2 Difference in simulated 3-h evaporative fraction (EF, %) at 0900 UTC (a), broad leaf fraction (%) (b) and water fraction (%) (c) between GLOB-ENS and CP-ENS. Top colourbar is shared between (a–c). (d) Observed climatological LST for April for reference of water body widths. (e) and (f) represent the 3-days accumulated precipitation ($\text{mm} \cdot 3 \text{ days}^{-1}$) for GLOB-ENS and CP-ENS, respectively over a Nigerian sub-domain (blue rectangle in (c)). Blue contours on (e and f) represent the inland water fraction (50% contour).



strictly separate the contributions of land and atmosphere to total ensemble rainfall spread. However, we hypothesise that on the morning after member initialisation, and in the absence of overnight rain, the initial SM spread dominates the spread in Day 1 morning turbulent fluxes, near-surface temperature and impacts on meso-scale circulations (cf Figure S3a–c) and afternoon rainfall.

The spatial patterns of ensemble spread in these variables are shown in Figure 3, also indicating pixels we excluded from subsequent analyses. First, we exclude

pixels where GLOB-ENS mean rainfall is zero on Day 1 of the forecast (masked grey) to ensure that the SM-rainfall feedback analysis is not influenced by regions where the atmosphere is too dry for rainfall, irrespective of surface forcing. We also remove individual member pixels where either rain prior to 0900 UTC exceeds 0.25 mm, or where incoming short-wave radiation is so low due to clouds ($<200 \text{ W m}^{-2}$) that morning EF anomalies are not representative of later in the day. Only pixels with ≥ 5 remaining ensemble members after applying these filters (Figure S1c,d) are considered. As expected

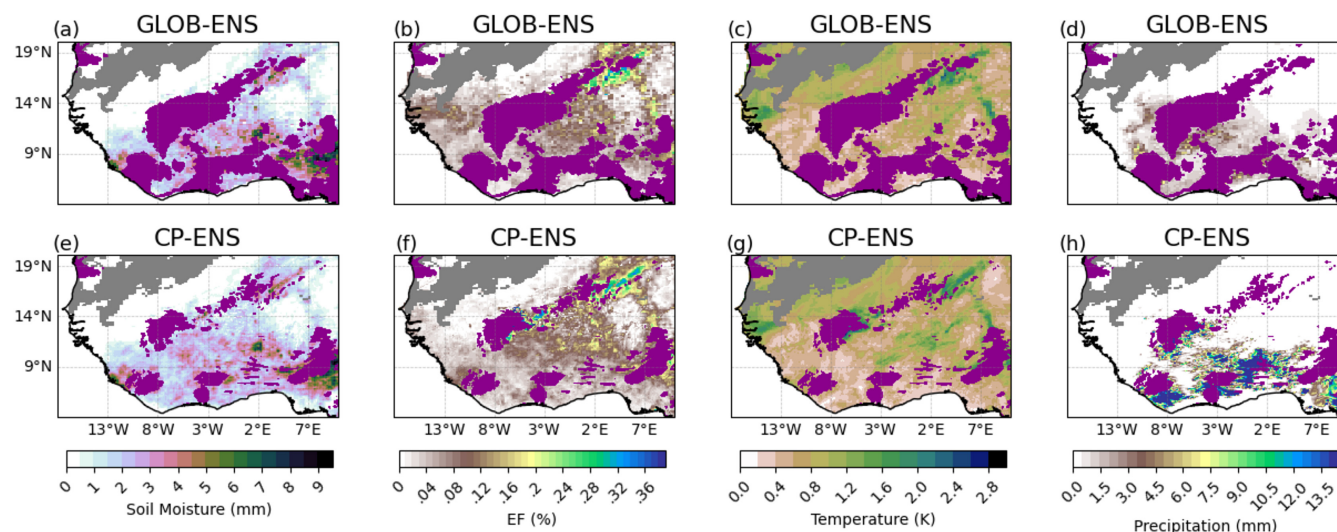


FIGURE 3 Standard deviation of initial soil moisture (mm) (a, e), and forecast Day 1 standard deviations of (b, f) 3-h evaporative fraction at 0900 UTC (%), (c, g) 1.5 m temperature (K) at 1000 UTC and (d, h) daily mean precipitation ($\text{mm}\cdot\text{day}^{-1}$) for GLOB-ENS and CP-ENS, respectively. Regions where all GLOB-ENS members simulate zero rainfall (grey), where ≥ 13 ensemble members exhibit ≥ 0.25 mm accumulated morning (0000–1000 UTC) rainfall, or where incoming short-wave radiation at 0900 UTC is $\leq 200 \text{ W}\cdot\text{m}^{-2}$ (dark purple) are masked and excluded from the analysis.

from the setup of CP-ENS, the spread in initial SM across members shows similar patterns for both ensembles (Figure 3a,e). This spread typically ranges between 2 and 5 mm, but reaches up to 10 mm where rainfall occurred in the Sahel in the previous day's forecast. The ensemble spread of pre-convective EF and near-surface temperature follow these SM patterns (Figure 3b,c,f,g), particularly across the Sahel (north of 9°N), where near-surface SM is known to have a strong control on surface flux partitioning and PBL temperatures (Lohou et al., 2014). Finally, Figure 3d,h illustrates the spread in afternoon rainfall for which sensitivity to initial SM conditions will be evaluated.

To quantify the coupling between initial SM, EF and near-surface temperature in both GLOB-ENS and CP-ENS, we calculate ensemble member anomalies for each variable relative to the ensemble mean for every valid pixel. Figure 4 shows the relationship between member anomalies of morning soil wetness and 1.5 m temperature. As it controls flux partitioning in the model, we express soil wetness as $(SM/SM_{crit})^2$, which shows an explained EF variance of 54% and 64% for GLOB-ENS and CP-ENS, respectively, reflecting the direct relationship between those two variables (Figure 4a,b). Figure 4d,e shows that the near-surface spread in the PBL is clearly affected by initial SM perturbations, with significant ($p \leq 0.05$) negative correlations between T1.5 m and $(SM/SM_{crit})^2$ anomalies. Both ensembles show a similar sensitivity of -8.0 K for GLOB-ENS and -7.3 K for CP-ENS per unit $(SM/SM_{crit})^2$, although the correlation is slightly weaker for CP-ENS

with an explained temperature variance (r^2) of 18.5% compared to 24.0% for GLOB-ENS. This is consistent with the CP model producing more PBL variability, for example, through transient mesoscale motions, which increase noise in snapshots of low-level temperature. The strength of land-atmosphere coupling follows a similar evolution over the 3-day forecasts in both ensembles. Figure 4c shows an average drop of 64% and 59% SM-explained variance in 1000 UTC EF over the 3-day forecast for CP-ENS and GLOB-ENS, respectively, illustrating the decay of initial SM perturbations. Strongest correlations between T1.5 m and $(SM/SM_{crit})^2$ anomalies occur each day around 0900–1000 UTC (Figure 4c,f). By this time of the morning, there has been sufficient surface heating to erode the nocturnal stable surface layer. A marked dip in r^2 occurs later in the day when convective clouds and rain develop, weakening the relationship between initial SM and surface fluxes. After sunset, when sensible heat flux is close to zero, the correlation with T1.5 m gradually weakens. The daytime dip in r^2 is more markedly pronounced in GLOB-ENS than CP-ENS. This is due to the increased frequency of rain in GLOB-ENS (Figure S2), effectively reducing the sensitivity of surface fluxes to initial SM. The rainfall maximum occurs 3 h earlier than in CP-ENS, consistent with previous studies (e.g., Cafaro et al., 2021; Pearson et al., 2014), and this weakens afternoon sensible heat fluxes (Folwell et al., 2022).

Having identified a significant effect of initial SM spread on near-surface temperature and EF, we now consider how the probability for afternoon rainfall changes

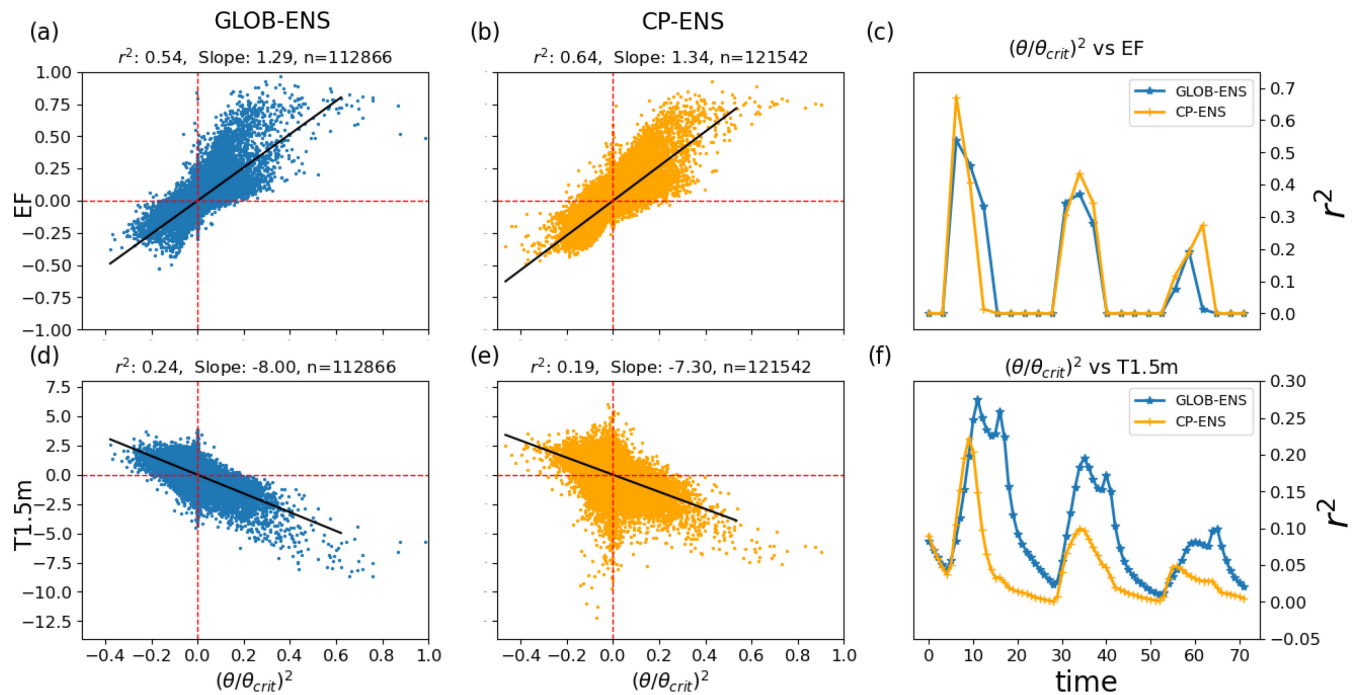


FIGURE 4 Scatter plots between initial $(SM/SM_{crit})^2$ and (a, b) 0900 UTC EF anomalies (%) and (d, e) 1000 UTC 1.5 m temperature anomalies (K) for GLOB-ENS and CP-ENS on Day 1 of the forecast. Anomalies are calculated relative to the ensemble mean. (c, f) show 3-day timeseries of explained variance (r^2) by initial $(SM/SM_{crit})^2$ for (c) EF anomalies, and (f) 1.5 m temperature anomalies. Relationships in (a, b), and (d, e) are shown for the day⁻¹ time of day when SM effects on the lower atmosphere are maximised, as illustrated in (c, f).

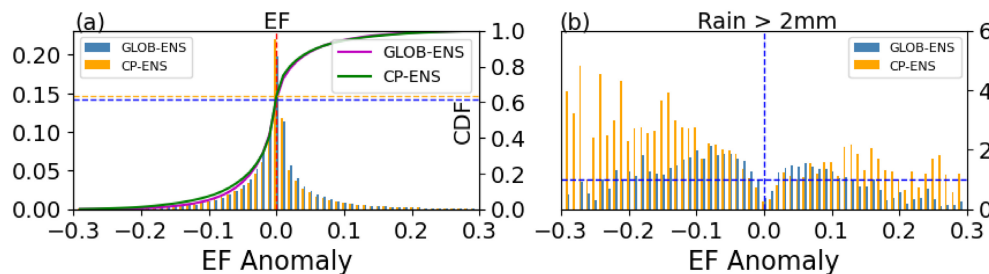


FIGURE 5 (a) Reference probability distributions (bars) and cumulative density functions (CDF, solid lines) of 0900 UTC EF anomalies based on all unmasked pixel-members for GLOB-ENS (blue, purple) and CP-ENS (orange, green) on forecast Day 1. Horizontal lines mark the probability for negative EF anomalies in both reference distributions according to the CDFs ($\sim 62\%$). (b) The probability distribution of afternoon rainfall >2 mm expressed as the ratio to the EF anomaly reference distributions (from (a)). A ratio above (below) 1 (dashed horizontal line) indicates an enhanced (suppressed) probability of rain for a given EF anomaly.

depending on co-located EF ensemble anomalies. Again we use the 0600–0900 UTC EF anomalies, filtered as above, and sampled across the domain and over all ensemble members. In Figure 5a, the frequency distribution of these EF anomalies (in bins of 0.01) is skewed towards drier conditions, with $61 \pm 1\%$ of all pixels showing a negative EF anomaly in both ensembles. This skewness reflects the nonlinearity in the relationship between SM and EF - flux partitioning becomes more sensitive to SM in drier regions. To assess how EF anomalies influence the likelihood of afternoon rain (after 1400 UTC), we plot the probability of rainfall accumulations

exceeding 2 mm within each EF bin (Figure 5b). A value above 1 indicates that rainfall occurs more frequently than would be expected based on the underlying EF frequency, while values below 1 imply rainfall is suppressed. CP-ENS shows values between 2 and 3 for almost all EF anomaly bins ≤ -0.1 , corresponding to around 10% of the distribution. This more than doubling in the likelihood of afternoon rain implies a robust negative coupling between initial SM perturbations and afternoon rain, as found in observations (Taylor, Gounou, et al., 2011). The frequency of >2 mm rainfall over the 25% driest EF anomalies of the reference distributions is 41% for

GLOB-ENS and 47% for CP-ENS, signifying a 64% and 88% higher frequency than expected for the 25% baseline, respectively. The markedly weaker dry-soil signal for GLOB-ENS is consistent with previous comparisons between simulations where convection is either parameterised or permitted (Hohenegger et al., 2009; Taylor et al., 2013), though we find rainfall to be more likely over negative EF anomalies for both ensembles.

4 | DISCUSSION AND CONCLUSION

Convection-permitting forecast systems promise to improve some of the major shortcomings of forecasts from coarser models that have to rely on convective parameterisations. This typically includes improved timing and intensity distributions for convective rainfall, as was shown for MOGREPS over East Africa (Cafaro et al., 2021), but similarly the potential for improved land-convection interaction. Here, we evaluated the effect of initial SM perturbations on near-surface ensemble

spread and rainfall probability in a first trial of Met Office convection-permitting MOGREPS forecasts (CP-ENS) over West Africa in comparison to its driving global ensemble (GLOB-ENS).

Our results for both models show that initial SM perturbations introduce considerable anomalies into daytime EF and near-surface temperatures, which are still evident on Day 3 of the forecast. Both models also show a tendency to a negative SM-precipitation feedback, with more frequent afternoon rainfall over low EF anomalies. However, this effect is much more pronounced in CP-ENS than GLOB-ENS. In addition, we identified persistent biases in rainfall caused by exaggerated areal coverage of water bodies in the GLOB-ENS setup, which is more realistically represented in CP-ENS.

We thus conclude that initial SM perturbations are an efficient way to introduce spread into low-level atmospheric conditions, lasting beyond 24 h lead time. Within the first 10 h and relative to the ensemble mean, we find widespread member EF anomalies above 0.1 and near-surface temperature anomalies reaching over 2°C locally. This near-surface response is particularly pronounced in the Sahel, which was also shown by Tennant and Beare (2014) in the first global trial of the MOGREPS SM perturbation scheme. They find an average increase in near-surface temperature spread of ~0.3°C for their 12-day forecast period, which we show here can be considerably higher locally on Day 1 of a forecast cycle.

The primary aim of the SM perturbation scheme is to counter the known under-dispersiveness of near-surface variables in the MOGREPS ensemble (Tennant & Beare, 2014).

Nevertheless, a correct process representation of the modelled rainfall response to SM perturbations is also an important factor as it affects deterministic skill (ensemble mean biases) as well as the SM-driven spread. For CP-ENS, we find a pronounced negative feedback between rainfall and SM-driven EF. GLOB-ENS on the other hand shows considerably lower dry-soil rainfall probabilities with a tendency to overall neutral behaviour to EF conditions. Given the comparable spread of near-surface variables in both ensembles, we assume this to be predominantly linked to the convective parameterisation used in the GLOB-ENS model setup. Such lower sensitivity to SM perturbations could cause an artificially smaller surface-driven rainfall spread in the global forecast system in comparison to CP-ENS, and contribute to ensemble underspread.

From a process-based perspective, GLOB-ENS seems to show a weaker representation of mechanisms that drive the observed negative SM feedback that dominates storm initiations and propagating storms across the Sahel, such as horizontal mesoscale circulations and (Klein & Taylor, 2020; Taylor, Gounou, et al., 2011). Consequently, GLOB-ENS likely underestimates rainfall probabilities over driest soils and negative EF anomalies, which would negatively affect its deterministic forecast and ensemble mean bias. Conversely, Tennant and Beare (2014) noted an improvement of forecast skill for convective rainfall over the British Isles for the convection-permitting regional MOGREPS when SM perturbations are introduced. Based on its dry-soil sensitivity found here, we would hence similarly expect an SM-linked reduction in real physical uncertainty for CP-ENS over West Africa, where convection is known to be more strongly controlled by SM conditions than in the mid-latitudes.

Our results illustrate how similar land perturbations can have different effects in forecast systems with explicit and parameterised convection, where the convection-permitting ensemble shows a more realistic representation of land-convection interaction than its global counterpart. Besides such process-based limitations however, the reliability of GLOB-ENS was additionally hampered here by exaggerated extents of water bodies, with persisting effect on rainfall patterns. This emphasises the need for careful evaluation of different mapping strategies for land cover.

Generally, ensemble forecast systems have to balance the aims of sufficient spread for improved probabilistic scores and of minimising overall ensemble bias. Focusing on ensemble spread, previous studies perturbed initial SM conditions by using different SM input datasets, concluding that SM perturbations can produce ensemble rainfall spread comparable to induced spread from atmospheric analyses perturbations (Maurer et al., 2015), and that convection-permitting models further increase near-surface spread

compared to coarser models, even for similar SM perturbations (Sutton et al., 2006). However, different from those studies, SM perturbations in MOGREPS are physically consistent with the scale and variability of rainfall patterns produced by the global forecast ensemble, which may result in smaller spread but allows the SM perturbations to contribute real physical forecast value. Tennant and Beare (2014) note that a further step for this physically consistent approach should be to use the SM perturbations produced by the convection-permitting model in the regional forecasts rather than interpolating perturbations from the global driving model. They find this high-resolution approach to further increase ensemble near-surface spread while decreasing the ensemble bias for a regional trial over Europe. Such results, together with the more realistic representation of land-convection relationships shown here, suggest a real potential for combined improvements in forecast ensemble spread and bias via implementation of realistic SM perturbations in convection-permitting forecast systems.

AUTHOR CONTRIBUTIONS

Valiyaveetil Shamsudheen Semeena: Conceptualization; data curation; formal analysis; methodology; validation; visualization; writing – original draft. **Cornelia Klein:** Conceptualization; methodology; supervision; writing – original draft. **Christopher M. Taylor:** Conceptualization; methodology; supervision; writing – original draft. **Stuart Webster:** Data curation; writing – review and editing.

ACKNOWLEDGEMENTS

This work was supported by UK Research and Innovation (UKRI) as part of the Global Challenges Research Fund, African Science for Weather Information and Forecasting Techniques (SWIFT) programme (NE/P021077/1). CK also acknowledges funding from the Natural Environment Research Council LMCS project (NE/W001888/1). Observational data used in this study is publicly available. IMERG data from the Global Precipitation Measurement mission are available from <https://doi.org/10.5067/GPM/IMERG/3B-HH/06> while EUMETSAT MSG Land surface temperature can be downloaded from <https://landsaf.ipma.pt/en/products/land-surface-temperature/lst/>. The MetOffice Unified Model forecast ensemble datasets can be made available upon request (semval@ceh.ac.uk).

CONFLICT OF INTEREST STATEMENT

The authors declare no conflict of interest.

ORCID

Valiyaveetil Shamsudheen Semeena  <https://orcid.org/0000-0002-1895-449X>

Christopher M. Taylor  <https://orcid.org/0000-0002-0120-3198>

REFERENCES

- Agustí-Panareda, A., Balsamo, G. & Beljaars, A. (2010) Impact of improved soil moisture on the ECMWF precipitation forecast in West Africa. *Geophysical Research Letters*, 37, XX–XX. Available from: <https://doi.org/10.1029/2010GL044748>
- Best, M.J., Pryor, M., Clark, D.B., Rooney, G.G., Essery, R.L.H., Ménard, C.B. et al. (2011) The Joint UK Land Environment Simulator (JULES), model description—part 1: energy and water fluxes. *Geoscientific Model Development*, 4, 677–699.
- Birch, C.E., Marsham, J.H., Parker, D.J. & Taylor, C.M. (2014) The scale dependence and structure of convergence fields preceding the initiation of deep convection. *Geophysical Research Letters*, 41, 4769–4776. Available from: <https://doi.org/10.1002/2014GL060493>
- Bowler, N.E., Arribas, A., Mylne, K.R., Robertson, K.B. & Beare, S. E. (2008) The MOGREPS short-range ensemble prediction system. *Quarterly Journal of the Royal Meteorological Society*, 134, 703–722. Available from: <https://doi.org/10.1002/qj.234>
- Bush, M., Allen, T., Bain, C., Boutle, I., Edwards, J., Finnenkoetter, A. et al. (2020) The first met Office unified model-JULES regional atmosphere and land configuration, RAL1. *Geoscientific Model Development*, 13, 1999–2029.
- Cafaro, C., Woodhams, B.J., Stein, T.H.M., Birch, C.E., Webster, S., Bain, C.L. et al. (2021) Do convection-permitting ensembles lead to more skilful short-range probabilistic rainfall forecasts over tropical East Africa? *Weather and Forecasting*, 36, 697–716.
- Crook, J., Klein, C., Folwell, S., Taylor, C.M., Parker, D.J., Stratton, R. et al. (2019) Assessment of the representation of west African storm lifecycles in convection-permitting simulations. *Earth and Space Science*, 6, 2018EA000491. Available from: <https://doi.org/10.1029/2018EA000491>
- Fletcher, J.K., Diop, C.A., Adefisan, E., Ahiataku, M., Ansah, S.O., Birch, C.E. et al. (2022) Tropical Africa's first testbed for high-impact weather forecasting and nowcasting. *Bulletin of the American Meteorological Society*, 1–27.
- Folwell, S.S., Taylor, C.M. & Stratton, R.A. (2022) Contrasting contributions of surface hydrological pathways in convection permitting and parameterised climate simulations over Africa and their feedbacks on the atmosphere. *Climate Dynamics*, 59, 633–648. Available from: <https://doi.org/10.1007/s00382-022-06144-0>
- Hagelin, S., Son, J., Swinbank, R., McCabe, A., Roberts, N. & Tennant, W. (2017) The met Office convective-scale ensemble, MOGREPS-UK. *Quarterly Journal of the Royal Meteorological Society*, 143, 2846–2861.
- Haiden, T., Rodwell, M.J., Richardson, D.S., Okagaki, A., Robinson, T. & Hewson, T. (2012) Intercomparison of global model precipitation forecast skill in 2010/11 using the SEEPS score. *Monthly Weather Review*, 140, 2720–2733. Available from: <https://doi.org/10.1175/MWR-D-11-00301.1>
- Hohenegger, C., Brockhaus, P., Bretherton, C.S. & Schär, C. (2009) The soil moisture-precipitation feedback in simulations with explicit and parameterized convection. *Journal of Climate*, 22, 5003–5020.
- Huffman, G., Stocker, E., Bolvin, D., Nelkin, E. & Tan, J. (2019) GPM IMERG Final Precipitation L3 Half Hourly 0.1 degree x 0.1 degree V06, Greenbelt, MD, Goddard Earth Sciences Data and Information Services Center (GES DISC). https://disc.gsfc.nasa.gov/datasets/GPM_3IMERGHH_06/summary
- Klein, C. & Taylor, C.M. (2020) Dry soils can intensify mesoscale convective systems. *Proceedings of the National Academy of*

- Sciences*, 117, 21132–21137. Available from: <https://doi.org/10.1073/pnas.2007998117>
- Koster, R.D., Dirmeyer, P.A., Guo, Z., Bonan, G., Chan, E., Cox, P. et al. (2004) Regions of strong coupling between soil moisture and precipitation. *Science*, 305, 1138–1140.
- Lohou, F., Kergoat, L., Guichard, F., Boone, A., Cappelaere, B., Cohard, J.-M. et al. (2014) Surface response to rain events throughout the west African monsoon. *Atmospheric Chemistry and Physics*, 14, 3883–3898.
- LSA SAF (2019) Land surface temperature climate data record—MSG, EUMETSAT SAF on land surface analysis. Technical Report. Available from: https://doi.org/10.15770/EUM_SAF_LSA_0001.
- Ma, Z., Zhao, C., Gong, J., Zhang, J., Li, Z., Sun, J. et al. (2021) Spin-up characteristics with three types of initial fields and the restart effects on forecast accuracy in the GRAPES global forecast system. *Geoscientific Model Development*, 14, 205–221.
- Martínez, I.R. & Chaboureaud, J.P. (2018) Precipitation and mesoscale convective systems: explicit versus parameterized convection over northern Africa. *Monthly Weather Review*, 146, 797–812.
- Maurer, V., Kalthoff, N. & Gantner, L. (2015) Predictability of convective precipitation for West Africa: does the land surface influence ensemble variability as much as the atmosphere? *Atmospheric Research*, 157, 91–107. Available from: <https://doi.org/10.1016/j.atmosres.2015.01.016>
- Maurer, V., Kalthoff, N. & Gantner, L. (2017) Predictability of convective precipitation for West Africa: verification of convection-permitting and global ensemble simulations. *Meteorologische Zeitschrift*, 26, 93–100.
- Parker, D.J., Blyth, A.M., Woolnough, S.J., Dougill, A.J., Bain, C.L., de Coning, E. et al. (2022) The African SWIFT project: growing science capability to bring about a revolution in weather prediction. *Bulletin of the American Meteorological Society*, 103, E349–E369. Available from: <https://journals.ametsoc.org/view/journals/bams/103/2/BAMS-D-20-0047.1.xml>
- Pearson, K.J., Lister, G.M.S., Birch, C.E., Allan, R.P., Hogan, R.J. & Woolnough, S.J. (2014) Modelling the diurnal cycle of tropical convection across the ‘grey zone’. *Quarterly Journal of the Royal Meteorological Society*, 140, 491–499. Available from: <https://doi.org/10.1002/qj.2145>
- Porson, A.N., Hagelin, S., Boyd, D.F., Roberts, N.M., North, R., Webster, S. et al. (2019) Extreme rainfall sensitivity in convective-scale ensemble modelling over Singapore. *Quarterly Journal of the Royal Meteorological Society*, 145, 3004–3022.
- Sobrino, J.A. & Romaguera, M. (2004) Land surface temperature retrieval from MSG1-SEVIRI data. *Remote Sensing of Environment*, 92, 247–254.
- Stephens, G.L., L’Ecuyer, T., Forbes, R., Gettleman, A., Golaz, J.C., Bodas-Salcedo, A. et al. (2010) Dreary state of precipitation in global models. *Journal of Geophysical Research Atmospheres*, 115, 1–14.
- Sutton, C., Hamill, T.M. & Warner, T.T. (2006) Will perturbing soil moisture improve warm-season ensemble forecasts? A proof of concept. *Monthly Weather Review*, 134, 3174–3189.
- Taylor, C.M., Birch, C.E., Parker, D.J., Dixon, N., Guichard, F., Nikulin, G. et al. (2013) Modeling soil moisture-precipitation feedback in the Sahel: importance of spatial scale versus convective parameterization. *Geophysical Research Letters*, 40, 6213–6218. Available from: <https://doi.org/10.1002/2013GL058511>
- Taylor, C.M., de Jeu, R.A.M., Guichard, F., Harris, P.P. & Dorigo, W.A. (2012) Afternoon rain more likely over drier soils. *Nature*, 489, 423–426. Available from: <http://www.nature.com/articles/nature11377>
- Taylor, C.M., Gounou, A., Guichard, F., Harris, P.P., Ellis, R.J., Couvreur, F. et al. (2011) Frequency of Sahelian storm initiation enhanced over mesoscale soil-moisture patterns. *Nature Geoscience*, 4, 430–433.
- Taylor, C.M., Parker, D.J., Kalthoff, N., Gaertner, M.A., Philippon, N., Bastin, S. et al. (2011) New perspectives on land-atmosphere feedbacks from the African monsoon multidisciplinary analysis. *Atmospheric Science Letters*, 12, 38–44.
- Taylor, C.M., Prigent, C. & Dadson, S.J. (2018) Mesoscale rainfall patterns observed around wetlands in sub-Saharan Africa. *Quarterly Journal of the Royal Meteorological Society*, 144, 2118–2132.
- Tennant, W. (2015) Improving initial condition perturbations for MOGREPS-UK. *Quarterly Journal of the Royal Meteorological Society*, 141, 2324–2336.
- Tennant, W. & Beare, S. (2014) New schemes to perturb sea-surface temperature and soil moisture content in MOGREPS. *Quarterly Journal of the Royal Meteorological Society*, 140, 1150–1160.
- Torn, R.D. (2010) Ensemble-based sensitivity analysis applied to African easterly waves. *Weather and Forecasting*, 25, 61–78.
- Vogel, P., Knippertz, P., Fink, A.H., Schlueter, A. & Gneiting, T. (2018) Skill of global raw and Postprocessed ensemble predictions of rainfall over northern tropical Africa. *Weather and Forecasting*, 33, 369–388. Available from: <https://doi.org/10.1175/WAF-D-17-0127.1>
- Vogel, P., Knippertz, P., Fink, A.H., Schlueter, A. & Gneiting, T. (2020) Skill of global raw and postprocessed ensemble predictions of rainfall in the tropics. *Weather and Forecasting*, 35, 2367–2385 <https://journals.ametsoc.org/waf/article/354676/Skill-of-Global-Raw-and-Postprocessed-Ensemble><https://journals.ametsoc.org/view/journals/wefo/35/6/WAF-D-20-0082.1.xml>
- Zipser, E.J., Cecil, D.J., Liu, C., Nesbitt, S.W. & Yorty, D.P. (2006) Where are the most: intense thunderstorms on earth? *Bulletin of the American Meteorological Society*, 87, 1057–1071.

SUPPORTING INFORMATION

Additional supporting information can be found online in the Supporting Information section at the end of this article.

How to cite this article: Semeena, V. S., Klein, C., Taylor, C. M., & Webster, S. (2023). Impact of land surface processes on convection over West Africa in convection-permitting ensemble forecasts: A case study using the MOGREPS ensemble. *Atmospheric Science Letters*, 24(8), e1167. <https://doi.org/10.1002/asl.1167>